J. Fluid Mech. (1986), *vol.* 166, *pp.* 341–358
Printed in Great Britain

On the interaction of small-scale oceanic internal waves with near-inertial waves

By D. BROUTMAN†
Department of Applied Mathematics and Theoretical Physics, University of Cambridge, Silver Street, Cambridge CB3 9EW

AND W. R. YOUNG
Department of Earth, Atmospheric, and Planetary Sciences, Massachusetts Institute of Technology, Cambridge MA 02139

(Received 28 February 1985 and in revised form 1 November 1985)

Ray theory is used to investigate the interaction of a short high-frequency progressive internal wave of infinitesimal amplitude with a long progressive near-inertial wave of arbitrary amplitude. Weak-interaction theory would, if applicable, predict that the largest changes in short-wave properties occur when the resonance condition $c = c_g$ is satisfied, where c is the phase velocity of the long wave and c_g is the group velocity of the short wave. The present calculation confirms this prediction only when the long wave has exceedingly small amplitude (peak velocities of order 0.1 cm/s).

However, when the background velocity has a realistic amplitude (e.g. oceanic values are of order 20 cm/s) the resonance condition fails to be relevant. For example, waves which initially have $c = c_g$ become trapped in low-shear regions and consequently experience very small changes in wavenumber. Other short waves, which initially have $c_g \ll c$ and hence violate the resonance condition, exhibit large and permanent changes in vertical wavenumber.

Remarkably, it is found that these permanent changes are much more likely to be decreases, rather than increases, in wavenumber. This can be explained as follows. Short waves which enter an inertial-wave packet experience both increases and decreases in wavenumber. However, at times when the wavenumber is relatively large, the group velocity is relatively small and the short wave is unlikely to escape from the inertial packet, whereas small wavenumber and large group velocity assist the escape of the short-wave group. Consequently the short waves that leave the inertial packet tend to have a smaller average wavenumber than those that enter. Thus the net effect of a near-inertial packet on a collection of short waves appears to be an increase in vertical wavelength and frequency.

1. Introduction

Near-inertial motions can strongly influence the propagation of internal waves of high frequency and short wavelength. The aim of this paper is to examine this interaction with a simple model. We consider the refraction, distortion, and amplification of a high-frequency, short-wavelength internal wave of infinitesimal amplitude (the 'test wave') by the velocity field of a single progressive wave of near-inertial frequency and arbitrary amplitude (the 'background wave'). Numerical and analytical solutions from ray theory form the basis of our approach.

† Present address: School of Mathematics, University of New South Wales, Kensington, N.S.W. 2033, Australia.

Descriptive studies of the oceanic internal wavefield characterize it as a quasi-continuous spectrum consisting of a random superposition of waves (e.g. Munk 1981). Correspondingly, many theoretical studies have been directed at predicting spectral properties using statistical closure methods (e.g. Olbers 1976; McComas & Bretherton 1977; Pomphrey, Meiss & Watson 1980; Meiss & Watson 1982). With the exception of Meiss & Watson (1982), the interacting waves in these studies are all assumed to have small amplitude. This is usually referred to as weak-interaction theory.

This paper adopts a different point of view in that it focuses on the particular interaction event described above, in which the near-inertial wave has finite amplitude. Despite the idealization involved in restricting attention to two waves, there are several reasons for pursuing this approach.

First, observations by Pinkel (1983) of the internal wavefield in the upper ocean (the first few hundred metres) show that near-inertial motions are vigorous. Moreover, only a few near-inertial-wave groups are present at any one time. T. B. Sanford (personal communication) has remarked that all of his upper-ocean Atlantic profiles, and most of his Pacific ones, are dominated by groups of downward-propagating inertial waves. If these measurements are representative of the upper ocean then in this region a continuous spectrum is as much an idealization as the model proposed here. In any case the present study provides some insight into how a downward-propagating group of near-inertial waves affects pre-existing smaller-scale waves.

Second, interest lies in understanding how the concept of an internal-wave critical layer (Booker & Bretherton 1967) is modified when the background flow is unsteady, in particular when it oscillates on inertial timescales. For the present model the vertical wavenumber of the test wave always remains bounded. In this sense critical-layer interactions do not occur. Nevertheless, it is possible for the wave action to become very large, and to do so at places and times which differ from those that would be predicted by a naive application of critical-layer theory.

Third, the idealization permits analytic results to be obtained, which serve to check the numerical solutions and enable a certain portion of parameter space to be surveyed. The analysis thus provides a convenient reference point for understanding the results of numerical simulations with different backgrounds, such as those of Broutman (1984) and Henyey & Pomphrey (1983).

A fourth motivation is the need to understand the limitations of weak-interaction theory, which has so far been the principal theoretical tool for studying nonlinearly interacting internal waves. The limitations have already been discussed by Holloway (1980, 1982). Here we can study the way in which weak-interaction theory breaks down by explicit illustration of some of the phenomena that accompany the breakdown. Our solutions also suggest an alternative view of transport through wavenumber space in the strong-interaction limit.

For instance, in the weak-interaction limit the induced-diffusion approximation (McComas & Bretherton 1977) yields the following prediction: the short wave interacts most strongly with the background, itself assumed weak, when

$$c_g = c, \tag{1.1}$$

where c_g is the vertical group velocity of the short wave and c is the phase velocity of the near-inertial wave. Physically, the interaction is most effective (for a sufficiently weak background) because a group of short waves is refracted by a shear that is approximately steady in its frame of reference. One of our principal conclusions is that (1.1) is not a reliable guide to which interactions are important, unless the background shear is unrealistically weak.

Indeed, the induced-diffusion mechanism, and other long-wave–short-wave interactions that can be described with weak-interaction theory, are generally obtained by assuming that the long wave, as well as the short wave, have sufficiently small amplitude. The ray approach used here is in some ways less restrictive: it permits stronger and more realistic shears (consistent with values measured in the ocean) in the velocity field of the long wave. Our strong shear solutions suggest a very different transport mechanism through wavenumber space, which has implications for our understanding of naturally occurring internal wavefields.

2. Ray solutions for an infinite progressive near-inertial wave

We consider a group of short internal waves propagating through a single progressive near-inertial wave. The choice of near-inertial frequency for the background wave simplifies the analysis: the ratio of horizontal to vertical wavelength is large for near-inertial motions so that the inertial current is approximately horizontal, circularly polarized, and independent of the horizontal coordinates.

If η denotes some property of the test wave (e.g. vertical displacement) then in the ray-theory approximation

$$\eta = a\, \mathrm{e}^{\mathrm{i}\theta}, \tag{2.1}$$

where $a(\boldsymbol{x}, t)$ is a local amplitude and $\theta(\boldsymbol{x}, t)$ is a phase function. The local wavenumber $\boldsymbol{k}$ and frequency ω are defined in terms of the wave phase by

$$\boldsymbol{k} = \nabla\theta, \quad \omega = -\frac{\partial\theta}{\partial t}, \tag{2.2}$$

with

$$\frac{\partial \boldsymbol{k}}{\partial t} + \nabla\omega = 0. \tag{2.3}$$

In a moving medium where the local velocity is $\boldsymbol{u}$, ω and $\boldsymbol{k}$ are related by

$$\omega = \boldsymbol{u}\cdot\boldsymbol{k} + \hat{\omega}(\boldsymbol{k}), \tag{2.4}$$

where $\hat{\omega}$ is the intrinsic frequency, which satisfies the internal-wave dispersion relation

$$\hat{\omega}^2 = \frac{N^2k^2 + f^2m^2}{k^2 + m^2}. \tag{2.5}$$

The axes are aligned so that $\boldsymbol{k} = (k, 0, m)$. In (2.5) N and f are the buoyancy and inertial frequencies respectively, assumed to be constant in the present study. The sign convection we adopt is that $\hat{\omega}$ is positive while wavenumbers may have either sign. For example, waves with negative vertical wavenumbers have negative vertical phase velocities but positive vertical group velocities.

The amplitude a is determined from action conservation:

$$\frac{\partial A}{\partial t} + \nabla\cdot[(\boldsymbol{u} + \boldsymbol{c}_{\mathrm{g}})\, A] = 0, \tag{2.6}$$

where $\boldsymbol{c}_{\mathrm{g}}$ is the group velocity,

$$\boldsymbol{c}_{\mathrm{g}} = \left[\frac{\partial\hat{\omega}}{\partial k}, 0, \frac{\partial\hat{\omega}}{\partial m}\right], \tag{2.7}$$

A is the action density,

$$A = E/\hat{\omega}, \tag{2.8}$$

and E is the intrinsic energy density. E is related to the amplitude of the vertical displacement field by

$$E = \tfrac{1}{2}\rho_0 N^2 a^2 \left[1 + \left(\frac{fm}{Nk}\right)^2\right], \tag{2.9}$$

where ρ_0 is the mean density.

2.1. *Solutions of* (2.3) *and* (2.6) *which are steady in the inertial-wave reference frame*

Suppose that the velocity field of the background inertial wave has the form

$$\boldsymbol{u} = [u(z-ct), v(z-ct), 0], \tag{2.10}$$

where c is the phase velocity. In the numerical calculations below we use a special case of (2.10):

$$\boldsymbol{u} = u_0[\cos b(z-ct), -\sin b(z-ct), 0], \tag{2.11}$$

i.e. a circularly polarized, vertically progressive inertial wave with vertical wavenumber b. Because the frequency of this background wave is near the inertial frequency, we have

$$c \approx f/b. \tag{2.12}$$

In much of the theoretical discussion below, it is simpler and more general to use (2.10), while (2.11) is used in the numerical calculations.

A general class of solutions of (2.3) and (2.6) is found by assuming θ and A to have the form

$$\theta = kx - \Omega t + \theta_1(z-ct), \quad A = A(z-ct), \tag{2.13a,b}$$

so that, from (2.2), m and ω also depend only on the combination $z-ct$. Then $\boldsymbol{k}$, ω, and A are steady in a frame of reference moving with the phase velocity c of the background inertial waves. Because m is a function of $z-ct$, (2.3) reduces to

$$\omega - cm = \Omega = \text{constant}, \tag{2.14}$$

where Ω is the absolute frequency of the short waves in the inertial-wave frame. Likewise (2.13b) simplifies (2.6) to

$$(c_g - c)\, A = \text{constant}, \tag{2.15}$$

where c_g is the z-component of $\boldsymbol{c}_g$. Much of our subsequent discussion is based on the fact that Ω in (2.14) is constant on a test-wave trajectory.

2.2. *Changes in vertical wavenumber as a function of* $z-ct$

If we adopt (2.11) as a specific model of the background velocity, then it is straightforward to contour Ω defined in (2.14) as a function of m and $\xi \equiv b(z-ct)/2\pi$ (figure 1). Because Ω is constant, a test wave released at any point in the (m, ξ)-plane remains on its initial Ω-contour. The immediate visual impression from figure 1 is that there are two types of initial conditions.

First, there are trajectories such as AA′ and BB′. These test waves propagate freely through the background wave and pass through all phase positions. Thus the test wave on AA′ has a positive group velocity which is always less than c. Consequently, it is repeatedly overtaken by upward-moving background crests. By contrast, the test wave on BB′ has a positive group velocity which is always greater than c. Consequently, this test wave repeatedly overtakes upward-moving background crests. Of course, test waves with positive wavenumbers (e.g. CC′) have negative group velocities and move downwards through the background wave.

Second, there are trajectories such as DD′ in figure 1. These test waves are

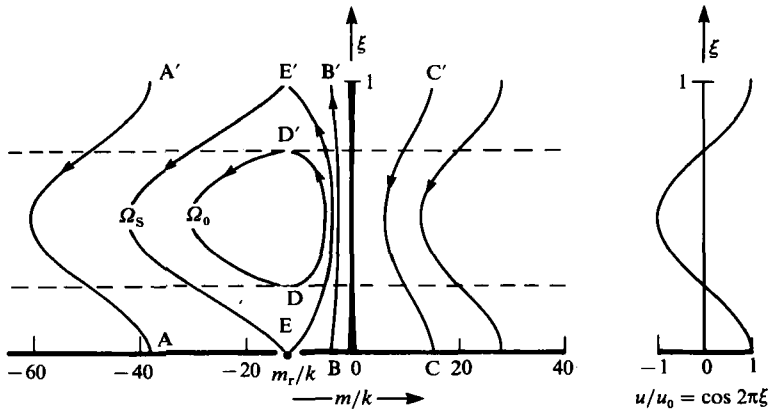

FIGURE 1. Contours of constant Ω in (m, ξ)-space. m_r is the resonant wavenumber at which (1.1) is satisfied. The horizontal dashed lines denote the phase positions where $u = 0$. The velocity of the inertial current as a function of the phase is shown at the right; $N/f = 75$, $b/k = 2.0$ and $J = (N/bu_0)^2 = 25$. The Ω-contours are computed using the mid-frequency approximation (2.19), except for those contours that closely straddle and cross the $m = 0$ axis. (These contours are computed using a high-frequency approximation for $\hat{\omega}$.) Note that the curves AA′ and BB′ have the same value of Ω. The test waves move along the Ω-contours in the direction shown by the arrows.

'blocked' when the background velocity exceeds a certain value u_b. Thus, in the figure, a test wave on the curve DD′ is confined to the region where background velocities are negative, i.e. for this particular wave $u_b = 0$. The contour for which $u_b = 0$ will be referred to as Ω_0. These test waves have $c_g > c$ when $m > m_r$ and $c_g < c$ when $m < m_r$. Thus on the right-hand portion of their orbit in figure 1, they overtake background-wave crests while on the left-hand portion they are overtaken. This is most clearly illustrated in the (z, t)-trajectory shown in figure 2. The turning points are caustics and occur at $m = m_r$ where (1.1) is satisfied. Equation (2.15) suggests that the action density is infinite at this resonant wavenumber but this is an unphysical singularity of ray theory which can be removed with a careful analysis of the caustic (Broutman 1986).

Analytic solutions for $m(z-ct)$, u_b and m_r can be obtained using a mid-frequency approximation, valid when $f^2 \ll \hat{\omega}^2 \ll N^2$. In this approximation, the dispersion relation (2.5) reduces to

$$\hat{\omega}^2 \approx \frac{k^2 N^2}{m^2}. \tag{2.16}$$

Substituting (2.16) into (2.14) leads to

$$m(z-ct) \approx \frac{1}{2c}\left[-(\Omega - uk) \pm [(\Omega - uk)^2 - 4Nkc]^{\frac{1}{2}}\right] \tag{2.17}$$

for $m < 0$. The positive root in (2.17) corresponds to $m > m_r$ and $c_g > c$, and the negative root to $m < m_r$ and $c_g < c$. At the turning point the two roots for m coalesce. Thus in the mid-frequency approximation

$$m_r \approx -\left(\frac{Nk}{c}\right)^{\frac{1}{2}}, \tag{2.18}$$

$$u_b \approx \frac{\Omega}{k} - 2\left(\frac{Nc}{k}\right)^{\frac{1}{2}}. \tag{2.19}$$

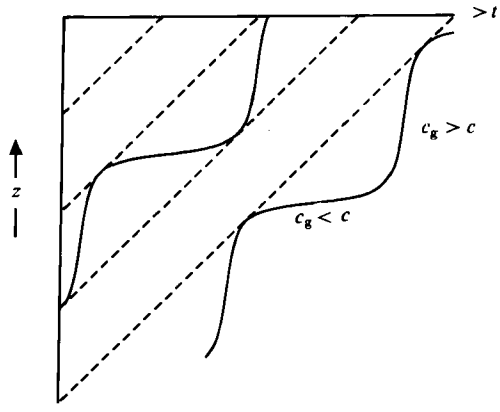

FIGURE 2. The vertical position z of a test wave as a function of time, computed from a numerical integration of the ray equations. The dashed lines are the phase positions of the inertial wave where $u = 0$. This test wave is on the orbit DD′ in figure 1.

2.3. *Extent of the region of closed Ω-contours*

The region of closed Ω-contours is bounded by the separatrix EE′. The value of Ω on this separatrix will be denoted by Ω_s. This region exists no matter how small the background velocity is, and its size increases as u_0 increases.

To make this more precise it is convenient to analyse (2.14) using the following non-dimensional variables:

$$m_* = \left(\frac{f}{Nkb}\right)^{\frac{1}{2}} m, \tag{2.20}$$

$$(\hat{\omega}_*, \Omega_*) = \left(\frac{b}{Nfk}\right)^{\frac{1}{2}} (\hat{\omega}, \Omega). \tag{2.21}$$

If we now apply the mid-frequency approximation (2.16), and use $c \approx f/b$, then

$$\Omega_* = |m_*|^{-1} - m_* + \mu \cos 2\pi\xi, \tag{2.22}$$

$$\mu = u_0 \left(\frac{bk}{Nf}\right)^{\frac{1}{2}}. \tag{2.23}$$

Further, it is easily shown that the resonant wavenumber, where (1.1) applies, is at $m_* = -1$.

This non-dimensionalization, and the mid-frequency approximation, leaves only one non-dimensional parameter: μ. Significantly, the only property of the test wave which affects μ is its horizontal wavenumber k. It is argued below that μ is a reliable estimate of the ability of the background shears to produce significant changes in the test-wave properties. Weak-interaction theory works in the limit of small μ, i.e. for sufficiently long *horizontal* test wavelengths.

This parameter is different from that advocated by Holloway (1980, 1982) as an *a priori* estimate of the validity of weak-interaction theory, which is

$$\nu \equiv \delta u / c_p, \tag{2.24}$$

where c_p is the horizontal phase velocity of the test wave and δu is the change in

background velocity which occurs in a vertical wavelength of the test wave. Using $\delta u \approx u_0 b/m$ and $c_p \approx N/m$ gives

$$\begin{aligned}\nu &= \frac{u_0 b}{N} \\ &= \{\text{Richardson number}\}^{-\frac{1}{2}} \\ &= \left(\frac{fb}{Nk}\right)^{\frac{1}{2}} \mu. \end{aligned} \tag{2.25}$$

The above provides a convenient way of estimating μ: oceanic Richardson numbers for inertial waves are order one, so

$$\mu \approx \left(\frac{Nk}{fb}\right)^{\frac{1}{2}} \tag{2.26}$$

and if $N/f = 75$ while $b = 2\pi/200m$, then

$$\mu = 8.7 \quad \text{if} \quad k = \frac{2\pi}{200m},$$

$$\mu = 3.9 \quad \text{if} \quad k = \frac{2\pi}{1000m},$$

$$\mu = 1.7 \quad \text{if} \quad k = \frac{2\pi}{5000m}.$$

Hence, realistic values of μ are order one or larger.

Now from (2.22) one can easily show that the value of Ω_* on the separatrix is

$$\Omega_{s*} = 2+\mu. \tag{2.27}$$

The size of the closed-contour region can be estimated by noting that the separatrix passes through the points

$$(m_*, \xi) = (-1 \pm (2\mu)^{\frac{1}{2}}, \tfrac{1}{2}) \quad \text{if} \quad \mu \ll 1, \tag{2.28}$$

$$(m_*, \xi) = (-(2+2\mu)^{\pm 1}, \tfrac{1}{2}) \quad \text{if} \quad \mu \gg 1. \tag{2.29}$$

If μ is small, the maximum width of the closed-contour region is proportional to $\mu^{\frac{1}{2}} \ll 1$. Thus $\delta m/m = O(\mu^{\frac{1}{2}})$ for the test waves in the closed-contour region. The test waves outside have much smaller changes in wavenumber: $\delta m/m = O(\mu)$. Thus, as suggested by the discussion surrounding (1.1), when $\mu \ll 1$, wavenumbers near m_r interact most strongly, but still weakly, with the background.

If μ is large, the width of the closed-contour region is roughly $2(1+\mu)$. In this realistic limit there are large fractional changes in wavenumber: $O(4(1+\mu)^2) \gg 1$. The region of closed contours is very large and is no longer centred on m_r. Most importantly, there is a broad range of wavenumbers, both inside and outside the separatrix, that interact strongly with the background. It is not possible to give a simple condition, analogous to $m = m_r$, which distinguishes strongly interacting test waves.

Finally, we emphasize that because of the simple form of the background velocity, all of the wavenumber changes discussed above are periodic. Permanent changes in wavenumber, which are indicative of transport through wavenumber space, occur when the background shear field is modulated and localized (§3).

3. Interaction with a group of inertial waves

In the previous section we obtained solutions of the ray equations by assuming that the (z,t)-dependence of the background current had the form $z-ct$. Thus for instance in figures 1 and 2 we confined our attention to the infinite wavetrain in (2.11). We now examine a localized near-inertial wave packet that is modulated by an envelope which travels at the group velocity of the near-inertial wave. In this case the background velocity is no longer steady in the inertial-wave frame because the phase velocity of the near-inertial wave differs from its group velocity. (In fact they have opposite signs.)

We consider a packet of near-inertial waves and replace (2.11) with

$$\boldsymbol{u} = u_0\, g(z-\alpha t)\,\{\cos b(z-ct),\ -\sin b(z-ct),\ 0\}. \tag{3.1}$$

The envelope is described by the function g and moves with the vertical group velocity α of the near-inertial waves. (If c is positive, α is negative.)

In the inertial-wave frame, the phase propagation of the near-inertial wave is brought to rest; however, the movement of the envelope is not stopped, so in this reference frame $\boldsymbol{u}$ varies with time. The time dependence gives rise to changes in Ω which can be computed from the ray equation

$$\frac{\mathrm{d}\Omega}{\mathrm{d}t} = k\left(\frac{\partial u}{\partial t} + c\,\frac{\partial u}{\partial z}\right), \tag{3.2}$$

where

$$\frac{\mathrm{d}}{\mathrm{d}t} = \frac{\partial}{\partial t} + \frac{\partial \hat{\omega}}{\partial m}\frac{\partial}{\partial z}. \tag{3.3}$$

For g we use the Gaussian profile

$$g = \mathrm{e}^{-(z/2L)^2}, \tag{3.4}$$

which has unit amplitude at the packet centre $z=0$ and vanishes as $z\to\pm\infty$. We have set $\alpha = 0$, consistent with an infinite horizontal wavelength and intrinsic frequency equalling f. The factor $2L$, where $L = 2\pi/b$, yields a slowly varying envelope containing about six or seven crests at any one time. The velocity u/u_0 at the time $t=0$ is plotted in figure 3. The minimum Richardson number of the packet is defined by

$$J = (N/bu_0)^2. \tag{3.5}$$

Throughout this section, N/f is set to 75 and b/k to 2.

The following results are produced by numerically integrating the ray equations

$$\frac{\mathrm{d}z}{\mathrm{d}t} = \frac{\partial \hat{\omega}}{\partial m}, \quad \frac{\mathrm{d}m}{\mathrm{d}t} = -k\,\frac{\partial u}{\partial z}. \tag{3.6a,b}$$

Unless otherwise stated, the ray integrations begin where $|u/u_0| = 0.0001$ (or $z \approx -6.1L$), so the test wave and the near-inertial packet are initially well separated. The integrations continue until the test wave emerges from the other side of the near-inertial packet.

Example 1 : *weak shears*, $J^{\frac{1}{2}} = 100$ *and* $\mu = 0.06$

Although near-inertial waves in the ocean generally produce shears that are strong enough to give minimum Richardson numbers of order unity, we shall first describe the case in which the inertial current is weak and has very large Richardson number, with $J^{\frac{1}{2}} = 100$. A weak current is an essential assumption of the weak-interaction theory, so we can compare the present results with induced diffusion to see if the two

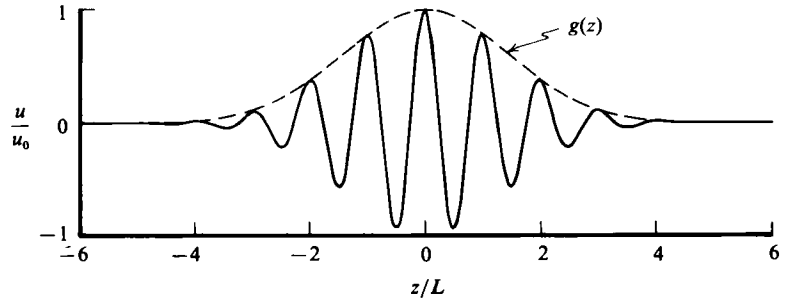

FIGURE 3. The profile at $t = 0$ of the x-component of the inertial current used in the computations of §3. The inertial packet is horizontally homogeneous, with $u/u_0 = g(z)\cos b(z-ct)$, $L = 2\pi/b$, $T = 2\pi/f$, and a Gaussian envelope of the form $g(z) = \mathrm{e}^{-(z/2L)^2}$.

agree qualitatively. (They cannot of course agree quantitatively.) In fact, if weak-interaction theory is to have any practical relevance to the problem at hand, it should do so here: rewriting (3.5) as

$$u_0 = \frac{N}{f}\frac{c}{J^{\frac{1}{2}}} \tag{3.7}$$

and using $N/f = 100$, $c = 100$ m/day (cf. Pinkel 1983), and $J^{\frac{1}{2}} = 100$ gives a value for u_0 of only 1 mm/s!

Figure 4 shows the time variation in m/k for four test waves with initial values $m/k = -8, -12.3, -15, -17$. The value of m_r/k, approximately -12.3 for $N/f = 75$ and $b/k = 2$, is indicated by the dashed line in the figure. Each time the test wave satisfies the resonance condition (1.1) the m/k curve crosses this line. In each integration Ω remains within a few percent of its initial value.

The test wave that starts with $m = m_r$ satisfies (1.1) at $t = 0$. This is equivalent to the resonant-triad condition of weak-interaction theory, in the induced-diffusion limit. This test wave undergoes larger fluctuations in m/k than the test waves that start with $m/k = -8$ and $m/k = -17$, neither of which ever satisfy condition (1.1). The largest changes in wavenumber, however, occur for the test wave with $m/k = -15$ initially, which satisfies (1.1) where $u/u_0 \approx 0.83$, near the centre of the inertial packet.

According to weak-interaction theory there can be an appreciable interaction when, initially, m is slightly different from m_r and c_g is slightly different from c. This is because a background wave with a small but finite amplitude and a slowly varying envelope implies a resonance band that is slightly broadened from a pure line. In our model, the region of closed Ω-contours (e.g. figure 1) identifies the most sizable interaction. More specifically, as will be demonstrated, test waves that orbit the outermost fringes of the closed contours have the greatest potential for the largest permanent change. Well within the closed-contour region, in the middle of the resonance band of weak-interaction theory, we often find minimal interaction because, as explained later, such test waves become securely trapped near the trough of the inertial wave. These different effects are much more pronounced in the following example.

Example 2: *strong shears*, $J^{\frac{1}{2}} = 2$ *and* $\mu = 3.06$

We next consider an example in which the inertial shear is increased to a strength more representative of values measured in the ocean. For $J^{\frac{1}{2}} = 2$ and $b/k = 2$ the test wave pictured in figure 5(*a*), with $c_g(t = 0) \approx 22c$, is among the fastest to be trapped

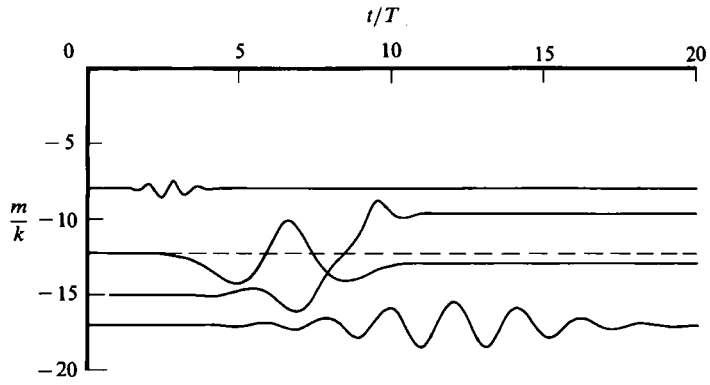

FIGURE 4. A comparison of the variations in m/k along the ray paths of four test waves. The results pictured here are for example 1 of §3 in the text. The horizontal axis is the time in inertial periods, with $T = 2\pi/f$. The dashed line is the resonant wavenumber m_r/k.

by the inertial wave; the test wave in figure 5 (*b*), with $c_g(t = 0) \approx 0.12c$, is among the slowest. Much smaller oscillations in wavenumber result when $c_g(t = 0) = c$, as illustrated by figures 5 (*c, d, e*) for three different initial positions of the test wave.

The magnitude of the wavenumber fluctuations experienced by a test wave depends on where, relative to the inertial wave, the test wave satisfies $c_g = c$ and becomes trapped. The test waves in figures 5 (*a, b*) require comparatively large inertial currents in order to refract to $c_g = c$ and $m = m_r$. Thus trapping occurs only toward the centre of the inertial packet, near a local maximum in u. While trapped, these test waves propagate through most of the phases of the inertial wave, analogous to a trajectory just inside the Ω_s contour of figure 1. Refraction then produces relatively large changes in wavenumber.

Initially, the test waves in figures 5 (*c, d, e*) meet the condition $c_g = c$ at $u = 0$. Upon entering the inertial packet, these test waves are quickly trapped by very weak inertial shears to depths where $u < 0$. The ray path of the test wave then oscillates about a single inertial-wave trough, where the trough is defined as a depth at which $\cos b(z - ct) = -1$. As the test wave propagates toward the centre of the inertial packet, the ray path remains trapped about this same inertial trough, and the weak shear required for trapping (and satisfying $c_g = c$) is encountered by the test wave at depths which approach the trough itself. In (m, ξ)-space, as in figure 1, the test wave then orbits a trajectory that lies well within the Ω_0 contour.

Thus test waves initially satisfying $c_g = c$ avoid strong refraction by settling into an inertial trough soon after they reach the inertial packet. They then ride through the inertial packet (at $c_g \approx c$) in phase with this trough and separated from regions of high inertial shear. While the test wave is trapped in regions where $u < 0$, it follows from (3.2) that its value of Ω decreases when the test wave is below the centre of the inertial packet and increases when the test wave is above the packet centre (figures 5 *c, d, e*).

The wavenumber fluctuations in figure 5 (*d*) are comparatively small because the test wave is initially positioned exactly on the trough of the inertial wave; the wavenumber fluctuations in figure 5 (*e*) are exceptionally large (for $c_g(t = 0) = c$) because the initial position of the test wave is near the inertial crest ($\cos b(z - ct) = 1$), at a depth where $\partial u/\partial z$ and dm/dt initially vanish. A test wave placed in this position can advance slightly farther into the inertial packet before refracting toward the inertial trough.

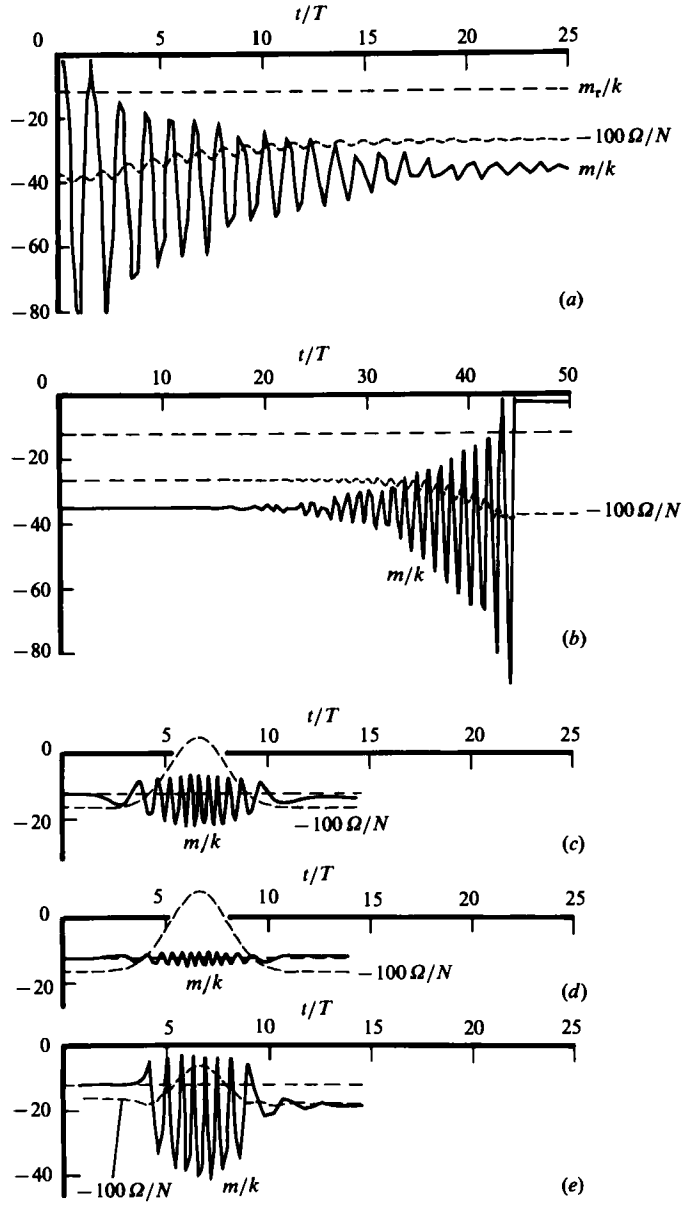

FIGURE 5. Variations in m/k and Ω as a function of time in inertial periods along the ray path of the test waves described in example 2 of §3. The initial values of m/k are -2.62 and -35.0 in (a) and (b) respectively. In (c, d, e) the initial wavenumber is $m = m_r$. The initial depths and times are (a, b, c) $z = -6.1L$, $t = 0$, (d) $-6.5L$, 0 and (e) $-6.1L$, $0.83T$.

These results provide a possible explanation for the failure of weak-interaction theory, whose prediction of the effect of long waves on short waves is the 'induced diffusion' of the latter in wavenumber space. The effect relied on to produce the diffusion is the resonance of the phase velocity of the long wave and the group velocity of the short wave. As examples 1 and 2 indicate, the conditions under which this phase-group resonance are important in our two-component model are considerably restricted and quite outside the range of conditions normally encountered in the

ocean. Although we have not considered random-phase inertial currents, which are essential for induced diffusion, the randomness of phase cannot change the limitation of weak-interaction theory in which the tuning of resonant triads is accurate to some small ϵ. This excludes triads (for two approximately equal values of $\boldsymbol{k}$) in which c_g is not close to c.

In the following subsection we show that a large and systematic net decrease in the magnitude of the vertical wavenumber of the test waves occurs in most encounters with a near-inertial packet when, initially, $c_g \ll c$ and hence when the resonance condition (1.1) is nowhere near satisfied.

3.1. *Permanent changes*

Permanent changes in m can be brought about through a net change in Ω; but our simulations indicate that Ω can be relatively constant even when there are dramatic changes in m. It is helpful, therefore, to consider the hypothetical example in figure 6 in which Ω is assumed to be constant along the ray trajectory.

In figure 6 we assign one plot of the type in figure 1 to each of four depths along the ray trajectory of the test wave as it traverses the near-inertial packet. In the inertial-wave frame these depths are labelled ξ_1–ξ_4, where $\xi = b(z-ct)/2\pi$. Plots of the local inertial velocity u/u_0 at each depth are also shown.

At the depth ξ_1 the test wave, propagating upwards in the inertial-wave frame, encounters the lower edge of the near-inertial packet. It has $\Omega = \Omega_t$ and initially $m > m_r$. (Note that m and m_r are negative.) The test wave therefore moves in the direction shown by the arrow along the Ω_t curve to the right of $m = m_r$ and to the right of the closed Ω-contours. (Since at a fixed depth Ω reaches a minimum at $m = m_r$, a consequence of (1.1), another Ω_t curve lies to the left of $m = m_r$ and, at $\xi = \xi_1$, to the left of the closed-contour region.)

As the test wave moves closer to the centre of the near-inertial packet, the region of the closed contours grows. At the depth ξ_2 the Ω_t contours pass across the saddle point to form the edge of the closed-contour areas. The test wave is now able to move along the Ω_t contour to values of $m < m_r$. For each complete circuit around the Ω_t curve, (1.1) is satisfied twice.

At the packet centre ($\xi = \xi_3$), the closed-contour region covers the widest range of wavenumbers. Above the packet centre this region shrinks again. Eventually the Ω_t contours become disjoint ($\xi_3 < \xi < \xi_4$). If $m < m_r$ at the time the Ω_t contour separates into two parts, then the test wave will emerge from the inertial packet at a larger $|m|$ than it had initially, moving downward in the wave frame, as shown by the arrow on the Ω_t contour in the uppermost plot.

The largest permanent changes are a consequence of the dispersion relation permitting two wavenumber solutions for each value of Ω. The two solutions are given by (2.17) in the mid-frequency approximation. Test waves satisfying $c_g = c$ somewhere in the inertial packet can pass from one wavenumber root to the other, as illustrated by figure 6.

As the test wave orbits a closed Ω-contour, it spends more time in the wavenumber range $m < m_r$ than in the range $m > m_r$. In figure 2, for instance, the test wave has $c_g < c$ more than three times as long as $c_g > c$. This would seem to indicate that the test waves are most likely to emerge from the inertial packet with $m < m_r$ and $c_g < c$. In fact, the opposite is true, especially for strong shears.

Before discussing why this is so, consider the results in figure 7, which shows ray trajectories for six initial values of m/k and five different starting times. Along each ray trajectory, (1.1) is satisfied at least once. Recall that the near-inertial packet, with $J = 4$ in this example, is centred at $z = 0$.

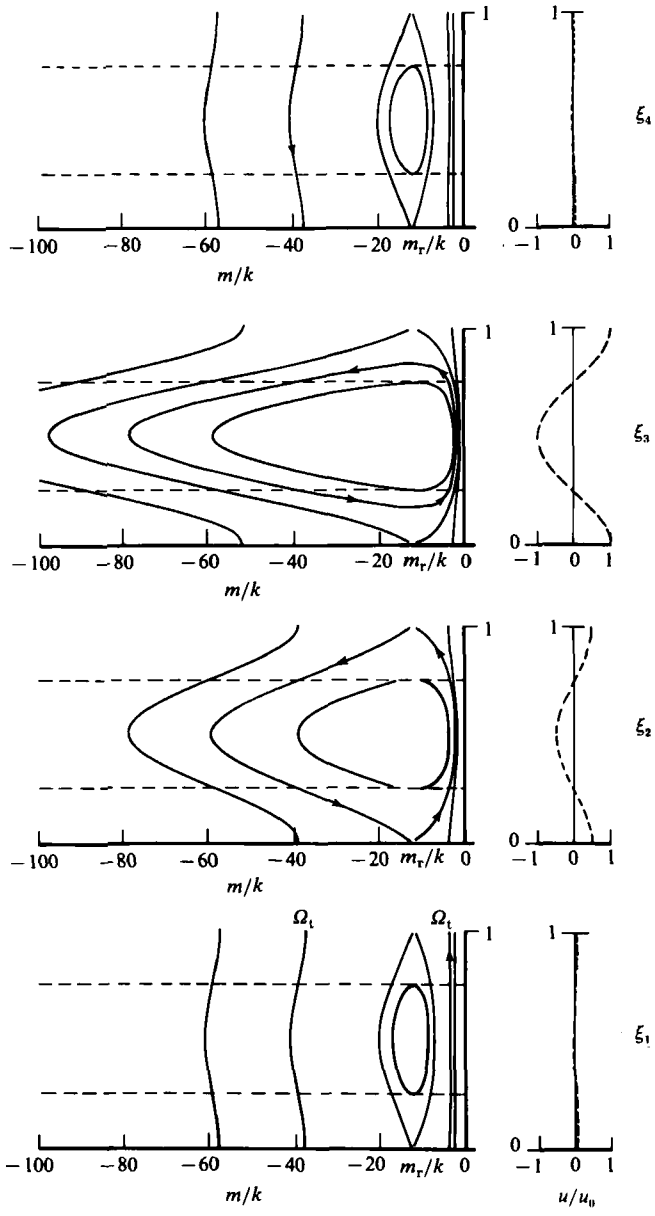

FIGURE 6. A plot of Ω-contours in (m, ξ)-space, as in figure 1, is here assigned to four depths across a near-inertial packet. The figure is meant to illustrate with a hypothetical example how a test wave encountering a near-inertial packet can experience a net change in wavenumber while conserving its value of Ω. The near-inertial packet is centred at ξ_3 and has a lower edge near ξ_1, and an upper edge near ξ_4. The values of Ω are computed using $J^{\frac{1}{2}} = 100, 4, 2, 100$ at ξ_1–ξ_4 respectively, and using u given in (2.11). The profiles of u/u_0 for the local value of $J^{\frac{1}{2}}$ are shown to the right, where u_0 is the maximum velocity at the packet centre. The test wave has $\Omega = \Omega_t$. These contours are labelled in the lower panel. In the other panels they are marked by arrows, which indicate the direction of propagation of the test-wave group in the inertial-wave frame.

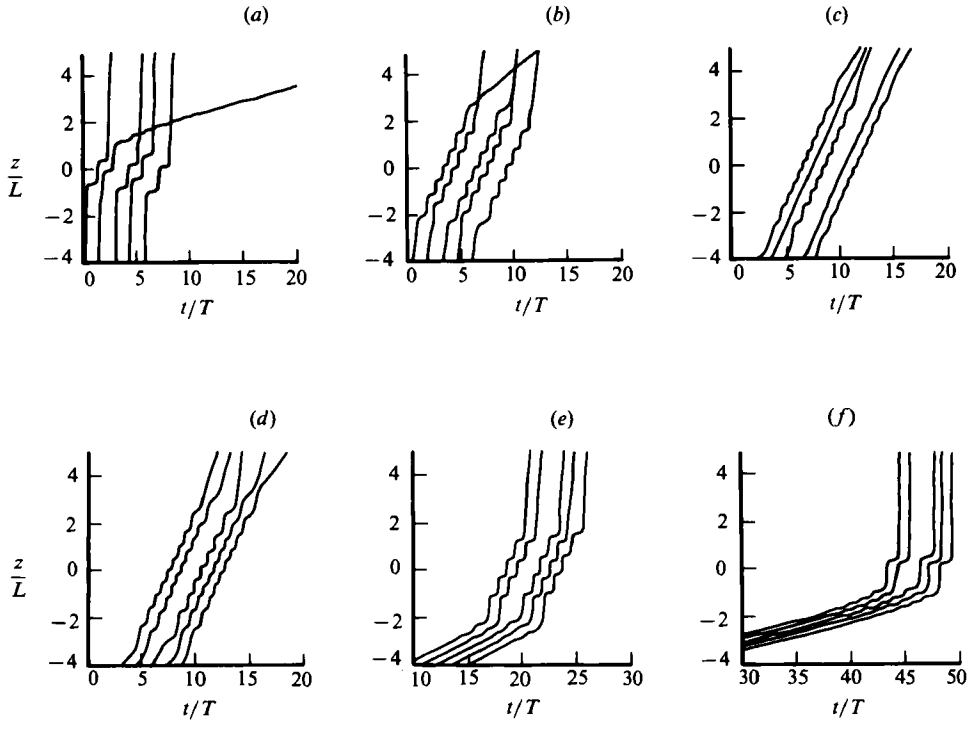

FIGURE 7. Ray trajectories for test waves propagating through a near-inertial packet. For each initial wavenumber there are five starting times spaced evenly over several inertial periods. Initial values are (a) $m/k = -3$; (b) $m/k = -6$; (c) $m = m_r$; (d) $m/k = -15$; (e) $m/k = -25$; (f) $m/k = -35$.

Test waves initially satisfying (1.1) are shown in the figure 7 (c). In this case the deflections in the ray path are relatively small in magnitude, especially with regard to the net effect of the encounter with the inertial packet. Much larger deflections in the ray path and much larger fluctuations in m occur when c_g and c differ by an order of magnitude. For example, the initial values of $m/k = -3$ (figure 7 (a)) and $m/k = -35$ (figure 7 (f)) correspond to initial group velocities of $c_g \approx 17c$ and $c_g \approx 0.12c$ respectively. Yet the refraction of these test waves can be seen to be comparatively large. Unlike the initially resonant test waves, these test waves are not trapped near an inertial-wave trough, but rather they propagate through more (but not all) of the phases of the inertial wave.

Moreover, in some cases there is a large permanent change in the direction of the ray path. This net change is most likely to occur when $c_g \ll c$ initially, as in the examples with the initial values $m/k = -25$ ($c_g \approx 0.24c$) and $m/k = -35$ ($c_g \approx 0.12c$). The reason for this becomes clear when contours of the inertial velocity are added to the plot of the ray trajectory. In figure 8 the ray trajectories are the same as those plotted in figure 7 (a). The dashed lines mark the position of the turning points, where (1.1) is satisfied and where $u = u_b$. The u_b contours are calculated from the initial value of Ω using (2.19).

Each time a ray trajectory encounters a u_b contour, it experiences a relatively sharp change in direction. When the ray is almost horizontal, the wavenumber is large and the group velocity is small. The short wave is thus unlikely to escape from the inertial packet without first encountering another u_b contour, at which it would be refracted

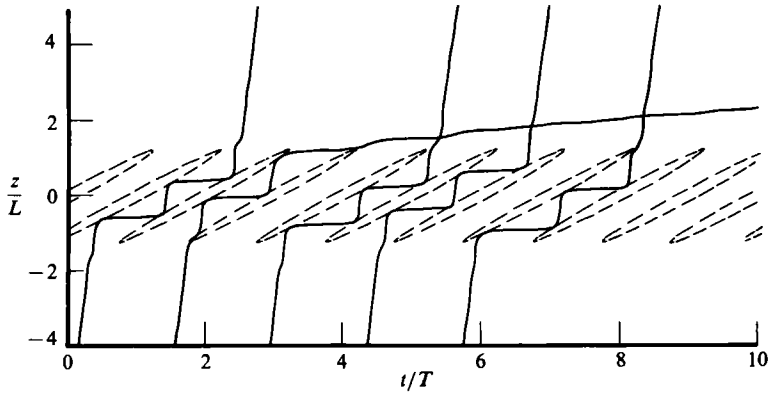

FIGURE 8. The ray trajectories in figure 7(*a*), with initial value $m/k = -3$, are redrawn here with the dashed curves showing the inertial phases where $u = u_b$, the velocity at which (1.1) is satisfied. The position of the u_b contours is approximate because u_b is computed using the *initial* value of Ω of the test wave and the mid-frequency estimate (2.19). For this example $u_b \approx 0.69u_0$. Note that the ray path is relatively straight until it approaches one of the u_b contours.

to low wavenumber and fast group velocity. The more horizontal the ray trajectory becomes, the stronger the tendency for test waves to emerge from the inertial packet with $|m| < |m_r|$ and $c_g > c$.

Note that these results suggest that *strong* interactions transport wave properties to *lower* wavenumbers, i.e. larger vertical scales. This is entirely contrary to the predictions of weak-interaction theory (viz. action is transported to high wavenumbers). For the idealized velocity fields discussed here, the physical mechanism is succinctly summarized in figure 8, which shows simply that low vertical wavenumbers have large vertical group velocities and consequently have the highest probability of escaping from spatially compact regions of high background shear. This effect is a simple and robust one, and is likely to apply to more complicated background fields.

4. Changes in energy

Permanent changes also occur in the intrinsic energy density E of the test waves, defined in (2.9), and in its integral $\int E\,\mathrm{d}V$, taken over a volume whose boundaries move at the local value of $(\boldsymbol{c}_g + \boldsymbol{u})$.

To determine the permanent change in the energy of the test wave, we designate the initial and final values of the test-wave parameters by the subscripts 1 and 2 respectively. These initial and final values occur away from the inertial packet, where the background medium is uniform and stationary. Then, because $\int A\,\mathrm{d}V$, the integrated action density, remains constant along the ray

$$\frac{\int E_2\,\mathrm{d}V_2}{\int E_1\,\mathrm{d}V_1} = \frac{\hat{\omega}_2}{\hat{\omega}_1}. \tag{4.1}$$

Since, as explained in §3, net increases in $\hat{\omega}$ are more likely to occur than net decreases, test-wave groups have a systematic tendency to increase their value of $\int E\,\mathrm{d}V$. This gain in energy of the test wave can only come at the expense of the inertial wavefield. Consequently, the interaction described here damps the downward-propagating group of inertial waves. A complete theoretical description of this damping mechanism requires a careful analysis correct to second order in test-wave amplitude.

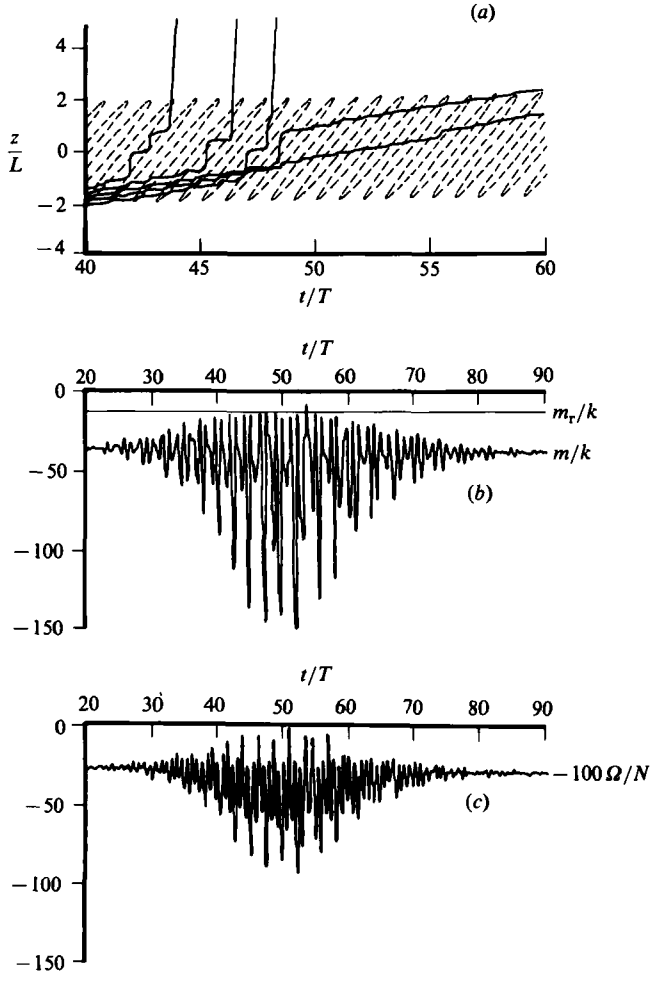

FIGURE 9. (*a*) The ray trajectories for test waves propagating through an inertial-wave packet containing upward- and downward-propagating inertial waves. Each near-inertial wave has a velocity of the form given by (3.1) and $J^{\frac{1}{2}} = 2$. The component with upward-moving phases has $b/k = 2$; the downward-propagating component has $b/k = 4$. The packet is modulated by the single Gaussian envelope g given in (3.4). Dashed contours are of $u_b \approx 0.41 u_0$ and are computed from the initial value of Ω of the test waves using (2.19). They indicate the approximate time and depths at which the test waves and the single progressive inertial wave with upward-moving phases satisfy (1.1). (*b*, *c*) The variations in m/k and Ω along the test trajectory in (*a*) that reaches $z \approx 2L$ at $t = 60T$. At $t = 0$ on each ray path, $m/k = -35$ and $z = -6.0L$.

Amplitude calculations are explored further in Broutman (1986), where an example is reported in which there is a large net increase in $\int E \, \mathrm{d}V$ but a net decrease in E and A because the group of test waves occupies a larger volume after interacting with the near-inertial packet.

5. Conclusion

The most surprising result to emerge from this study is the tendency for a downward-propagating, near-inertial-wave group to permanently decrease the magnitude of the vertical wavenumber of upward-propagating short-wave groups.

This is clear from figure 8 and from many other examples that we have run: most test waves with small wavenumbers pass through the packet without any marked change, while most of those with initially high wavenumbers emerge with much smaller wavenumbers and faster group velocities. As already indicated in figure 8 this is because, when the wavenumber is small, the group velocity is large and the test wave has the greatest probability of escaping from the background shear field.

Is this mechanism operating in the ocean? Because it relies on the presence of groups of inertial waves, such as are found in the upper ocean, we suggest that the upper ocean is the most likely site. For example, Pinkel's (1983) Doppler sonar observations suggest that much of the shear in the upper 700 m of the ocean can be attributed to a few identifiable groups of downward-propagating near-inertial waves.

It might be objected that actual background fields, even in the upper ocean, are probably not as narrowband as those used here. However, Flatté, Henyey & Wright (1985) have remarked that in their numerical simulations, where the background is constructed from a Garrett–Munk spectrum using a random phase approximation, there is a clear statistical tendency for the vertical wavenumber to decrease. This independent result is encouraging, but without a detailed study of actual events it is difficult to see whether this decrease can indeed be attributed to the mechanism in figure 8. However our impression is that the process is robust, in that it is not disrupted if the background is made more complex.

Thus, for example, in figure 9 we show five test waves propagating through a packet of near-inertial waves containing upward- and downward-propagating components and modulated by a stationary Gaussian envelope. Clearly Ω is not even approximately constant in this case, and consequently the contours of u_b, based on the theory of §2, are no longer a reliable guide to the position of the turning points. Nonetheless, figure 9 shows that the conversion from high to low wavenumbers still occurs. This example, as well as several others we have performed, suggests that spatial compactness of the high-shear region is more essential than a single harmonic structure within it. The time dependence of the background flow is also important for this phenomenon; it removes the constraint that the absolute frequency $\hat{\omega}+ku$ be constant along the ray. In a steady horizontal shear flow this constraint forces $\hat{\omega}$ to return to the same value whenever $u = 0$, preventing permanent changes of the type described here. The time dependence of the oscillating inertial current also eliminates critical layers, which would otherwise be important for short-wave dynamics.

D.B. received funding from the Natural Environment Research Council (grant GR3/4747) and benefitted from discussions with Dr M. E. McIntyre on many aspects of this study. Input from Dr Greg Holloway and the referees is also appreciated. W. R. Y. received funding from ONR grant N00014-79-C-0472.

REFERENCES

Booker, J. R. & Bretherton, F. P. 1967 The critical layer for internal gravity waves in a shear flow. *J. Fluid Mech.* **27**, 513–539.

Broutman, D. 1984 The focusing of short internal waves by an inertial wave. *Geophys. Astrophys. Fluid Dyn.* **30**, 199–225.

Broutman, D. 1986 On internal-wave caustics. *J. Phys. Oceanogr.* (in press.)

Flatté, S. M., Henyey, F. S. & Wright, J. A. 1985 Eikonal calculations of short-wavelength internal-wave spectra. *J. Geophys. Res.* **90**, 7265–7272.

HENYEY, F. S. & POMPHREY, N. 1983 Eikonal description of internal wave interactions: a non-diffusive picture of "induced diffusion". *Dyn. Atm. Oceans* **7**, 189–219.

HOLLOWAY, G. 1980 Oceanic internal waves are not weak waves. *J. Phys. Oceanogr.* **10**, 906–914.

HOLLOWAY, G. 1982 On interaction time scales of oceanic internal waves. *J. Phys. Oceanogr.* **12**, 293–296.

MCCOMAS, C H. & BRETHERTON, F. P. 1977 Resonant interaction of oceanic internal waves. *J. Geophys. Res.* **82**, 1397–1422.

MEISS, J. D. & WATSON, K. M. 1982 Internal-wave interactions in the induced-diffusion approximation. *J. Fluid Mech.* **117**, 315–341.

MUNK, W. H. 1981 Internal waves and small-scale processes. In *Evolution of Physical Oceanography* (ed. B. A. Warren & C. Wunsch), p. 623. MIT Press.

OLBERS, D. J. 1976 Nonlinear energy transfer and the energy balance of the internal wave field in the deep ocean. *J. Fluid Mech.* **74**, 375–399.

PINKEL, R. 1983 Doppler sonar observations of internal waves: wavefield structure. *J. Phys. Oceanogr.* **13**, 804–815.

POMPHREY, N., MEISS, J. D. & WATSON, K. M. 1980 Description of nonlinear internal wave interactions using Langevin methods. *J. Geophys. Res.* **85**, 1085–1094.